

Konstruiranje izdelka s pomočjo tehnike optimizacije stika

Product Design Using a Contact-Optimization Technique

István Páczelt - Attila Baksa - Tamás Szabó
(University of Miskolc, Hungary)

Znano je, da v inženirski praksi nastajajo velike napetosti zaradi oblik in obremenitev teles v stiku. Porazdelitev napetosti običajno ni enakomerna, singularnosti pa skrajšujejo dobo trajanja strojnih elementov. Zato je pomembno z ustreznim oblikovanjem stikov odpraviti omenjene singularnosti. Eden od ciljev prispevka je predstavitev metode, ki rešuje problem singularnosti v stikih. Z nadzorom dotikalnega tlaka lahko dosežemo enakomerno porazdelitev dotikalnega tlaka. Postopek optimizacije upošteva mejne napetosti materiala. V prispevku obravnavamo dva tipa dotikalnih problemov. Najprej analiziramo dotikalne probleme s predpostavko o linearni elastičnosti in majhnih deformacijah ter ustaljeno obrabo. Dva numerična primera pojasnjujeta ta postopek. Obravnavani so tudi parametri nadzorne funkcije, ki omogoča največjo nosilnost, kar je uporabno za konstruiranje zavor in ležajev. V drugem delu prispevka obravnavamo rešitev dotikalnih problemov za velike pomike in deformacije. Za primer je značilna vzmet, pri kateri primerjamo računске vrednosti krivulje nelinearnega pomika z rezultati meritev.

© 2007 Strojniški vestnik. Vse pravice pridržane.

(Ključne besede: metode končnih elementov, konstruiranje izdelkov, optimiranje stika, iteracije)

It is well known that in engineering practice high stresses occur and that these stresses depend on the shapes and the loads of the bodies in unilateral contact. The stress distribution is often not smooth and has some singularities, thereby decreasing the lifetime of the machine elements. It is an important objective to obtain a smooth stress distribution when optimizing the shape of the elements. One of the goals of this paper is to present a method that resolves the above problem. By controlling the contact pressure a prescribed, smooth contact-pressure distribution can be achieved. The optimization problems take into account the limit stress constraints of the material. In the present paper two types of contact problems are investigated. Firstly, contact optimization problems are analyzed assuming linear elasticity and small displacements, including steady-state wear process. Two numerical examples are presented on this topic for a rolling machine element: a punch optimization and a shape optimization. We also investigated which parameter values of the controlling function result in the maximum loadability. This can be useful in the design of brakes or bearings. In the second part of the paper the solution of the contact problem for large displacements and deformations is investigated where an air-spring is analyzed by calculating the nonlinear load-displacement curve and comparing it with measurements.

© 2007 Journal of Mechanical Engineering. All rights reserved.

(Keywords: finite element methods, product design, mechanical contacts, contact optimization, iterative methods)

0 INTRODUCTION

In engineering practice, connections between machine elements are frequently modeled as unilateral contact problems. Comparatively few studies can be found in the literature for contact optimization [1]. Nevertheless, a thorough mathematical investigation of the subject can be found in [2], and in [3] the contact problems of wearing processes are investigated in an analytical way.

The elimination of stress singularities is an important engineering task. In order to overcome this problem, the application of contact-pressure control is recommended, since this ensures a smooth contact-pressure distribution as well as a zero value on the part of the border of the contact zone.

The papers [4] to [6] provide solutions for 2D and 3D problems in which the contact-pressure distribution is partially controlled by minimizing the maximum contact pressure. The authors of [6]

took into account the stress limit in the case of solving contact-optimization problems for axially symmetrical bodies. The equivalent von Mises stress σ_e must be under a prescribed limit (σ_p). The present paper extends the load cases for the examined numerical examples; in addition to the external force load here the kinematical loads can also be applied on the contacting particles. Discretization of the domain with p -version finite elements is advantageous [7], since it results in rapid convergence, and high-order mapping ensures an accurate geometry for the shape optimization.

The lifetime of a roller bearing is influenced by many parameters, e.g., the type and the shape of the rollers, the number of rows, the shapes of the tracks of the bearing rings, the bearing dimensions, the materials and their treatment, the quality of manufacturing, etc. A number of papers, e.g., [8] to [13] are devoted to the issue of the roller's rounding-off. In these papers, except the last one, the radius of the rounding-off that results in a generally non-smooth contact pressure distribution is given.

Different rounding-off techniques, e.g., cylindrical or conical rollers, have rounding-off with a given radius at the ends, but it is also possible to make rounding-off a logarithmic function of radius, as published in [14] and [15]. The problem of rounding-off is also analyzed in case of elasto-hydrodynamic lubrication in [16] and [17]. The question of rounding-off is examined in references [4] and [6] for roller bearings without restrictions for the stress limit. The constraint for the equivalent stress limit is not taken into account in the papers referenced above, but due to the loadability it is required.

In the present paper the equivalent stress limit is considered through the optimization process as a constraint. The optimal shape is achieved by an iteration-based algorithm (see [18]). A numerical example is presented in Section 2.6.

Sub-section 2.3 of this paper deals with the wear problem of the relative sliding of two contacting bodies. The transmittable torque with a clutch and frictional power loss in the case of brakes are important quantities during the design process, and due to wear the shapes of the bodies are changing. There are numerous algorithms to describe the transient wear process ([19] to [21]). These algorithms have huge processing-time requirements. There is also the question of how we can determine the shape of the bodies and the

contact pressure distribution in the case of steady-state wear without using the algorithms for a time-dependent wear process. One investigation [18] suggests a technique for the previous problem. The present paper gives a formulation for calculating the wear of disk brakes in steady-state based on the modified Archard law.

Recently, the classical springs used in vehicles for suspension have been replaced by air-springs. The advantage of an air-spring compared to a classical spring is its nonlinear behavior, which can be controlled by the inflation pressure. In addition to the force displacements of the diagram, the designer is interested in determining the stresses and strains in the reinforcing fibers. Accurate results can be obtained by a p -extension of the finite-element method, but its application for problems with large displacements requires much more work. Therefore, a simplification is performed, i.e., the contacting element sides are kept in a straight line, which made it possible to use the algorithm given by Crisfield [22] for the h -extension elements. A numerical example is presented in Section 4 to demonstrate the working process of an air-spring.

1 TREATMENT OF THE CONTACT

Without the restriction of generality let us consider the contact problem of two elastic bodies ($\alpha = 1, 2$). The surfaces of the bodies are separated into three regions: S_u^α denotes the part of the body where displacements u_0 are given, in S_t^α the traction t_0 is applied, while S_c^α represents the part of the bodies where the contact is expected. The S_c^α part of the body is called the proposed zone of the contact. The bodies are loaded with the body force b^α . We are interested in finding the displacement vector field u^α , the strain A^α and stress T^α tensor fields.

1.1 Contact kinematics

The contacting surfaces are described in parametric form (see [23]): The contacting surface of the body labeled $\alpha = 1$ (or $\alpha = 2$) is written in terms of the parameters ($\xi = (\xi^1, \xi^2)$) (or $\eta = (\eta_1, \eta_2)$). In the implementation the parameters will be associated with the element surfaces using optimal approximations based on the Babuška points.

Let $X^1(\xi)$ and $X^2(\xi)$ represent the possible contact points of bodies 1 and 2, respectively, in

the reference coordinate system. The position vectors of these points at time t can be written in terms of the displacement $\mathbf{u}^1(\xi, t)$ for body 1:

$$\mathbf{x}^1 = \mathbf{x}^1(\xi, t) = \mathbf{X}^1(\xi) + \mathbf{u}^1(\xi, t) \quad (1)$$

and similarly for body 2:

$$\mathbf{x}^2 = \mathbf{x}^2(\eta, t) = \mathbf{X}^2(\eta) + \mathbf{u}^2(\eta, t) \quad (2),$$

where $\mathbf{u}^2(\eta, t)$ is the displacement function of body 2. Therefore, the gap between the two bodies is given by:

$$(\mathbf{x}^2 - \mathbf{x}^1) \cdot \mathbf{n}_c \geq 0 \quad (3),$$

where \mathbf{n}_c is normal to body 1 at point \mathbf{x}^1 and intersects body 2 at point \mathbf{x}^2 . The minimum distance between a fixed point of body 2 corresponding to parameter η and body 1 is given by

$$|\mathbf{x}^2(\eta, t) - \mathbf{x}^1(\xi, t)| = \min_{\xi} |\mathbf{x}^2(\eta, t) - \mathbf{x}^1(\xi, t)| \quad (4).$$

The points corresponding to body 1 that satisfy Equation will be identified by an overbar in the following: $\bar{\mathbf{x}}^1 = \mathbf{x}^1(\bar{\xi}, t)$ and the corresponding normal will be denoted by $\bar{\mathbf{n}}_c$, see Figure 1.

The inequality constraint of the non-penetration condition is defined as:

$$d = (\mathbf{x}^2 - \bar{\mathbf{x}}^1) \cdot \bar{\mathbf{n}}_c \geq 0 \quad (5)$$

and the penetration function for the penalty method is written as:

$$d^- = \begin{cases} (\mathbf{x}^2 - \bar{\mathbf{x}}^1) \cdot \bar{\mathbf{n}}_c & \text{if } (\mathbf{x}^2 - \bar{\mathbf{x}}^1) \cdot \bar{\mathbf{n}}_c < 0 \\ 0 & \text{otherwise} \end{cases} \quad (6).$$

1.2 Contact conditions

The normal stress along the surface $S_c^\alpha = \Omega$ is $\sigma_n^\alpha = \mathbf{n}^\alpha \cdot \mathbf{T}^\alpha \cdot \mathbf{n}^\alpha$, where \mathbf{n}^α is the outer normal of the body α , \mathbf{T}^α is the stress tensor and ' \cdot ' means the scalar product. For small displacements after the deformation the gap can be calculated as $d = u_n^2 - u_n^1 + g$, where $u_n^\alpha = \mathbf{u}^\alpha \cdot \mathbf{n}_c$ and g is the initial gap. By introducing the notation of contact pressure $p_n = -\sigma_n^1 = -\sigma_n^2$ there is contact if $d = 0, p_n \geq 0, \mathbf{x} \in \Omega_p$ and there is gap if $d > 0, p_n = 0, \mathbf{x} \in \Omega_g$, i.e. $p_n \cdot d = 0, \mathbf{x} \in \Omega = \Omega_p \cup \Omega_g$.

Coulomb dry-friction models are examined henceforth. The boundary value problem is solved by variational principles using a modified complementary energy and the total potential energy with an augmented Lagrangian technique ([4] and [23]).

1.2.1 Control of the contact pressure

The resulting contact stress distribution and, therefore, the contact pressure, are mainly influenced by the shape of the bodies that are in contact, and the initial distance between them. The aim is to ensure the contact of the bodies on a sub-

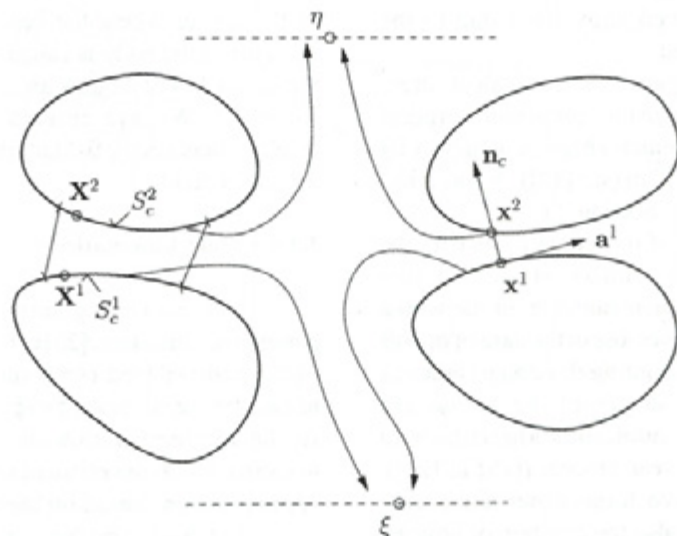


Fig. 1. Notation

domain, indicated by Ω_c (here is only a line), and on that contact surface the pressure varies as a prescribed function. This is achieved by the modification of the shape of the contacting parts. The rest of the supposed contact domain $S_c = \Omega$, which is Ω_{nc} where the pressure distribution is not known, but it must be less than a prescribed function.

In our optimization problems it is supposed that the bodies are in contact on the whole sub-domain Ω_c of the contact zone $S_c = \Omega$. The contact surface is modified in a way that the following function holds true for the contact pressure

$$p_n(\mathbf{x}) = v(\mathbf{x}) p_{\max}, \quad \mathbf{x} \in \Omega_c = [s, t = 0] \quad (7),$$

where the chosen control function must satisfy the condition $0 \leq v(\mathbf{x}) \leq 1$, and

$$p_{\max} = \max p_n(\mathbf{x}), \quad \mathbf{x} = [s, t] \quad (8),$$

where s and t are surface coordinates in the region Ω_c . In the sub-domain $\Omega_{nc} = (\Omega = \Omega_c \cup \Omega_{nc})$ the fulfillment of the following inequality is required

$$\chi(\mathbf{x}) = v(\mathbf{x}) p_{\max} - p_n(\mathbf{x}) \geq 0, \quad \mathbf{x} \in \Omega_{nc} \quad (9).$$

The definition of the control function is arbitrary. In order to avoid the singularities in the

stress distribution practically, it is defined in such a way that not only the value of the function must be zero at the end of the control zone but also the first derivative in a sort of direction as well.

Therefore, let us define a function $v(s)$ of class C^1 in the sub-region Ω_c (see Figure 1). The normal shape variation is assumed to be specified by a function $v(s)$ of class C^1 in the sub-region Ω_c . We introduce the functions depending on the coordinate s :

$$V^*(s) = f_2 + (f_3 - f_2) \frac{s - L_2}{L_3 - L_2} \quad (10)$$

$$f_2 \geq 0, f_3 \geq 0$$

and

$$V(s) = 0,$$

$$V(s) = V^*(s) \left\{ 3 \left(\frac{s - L_1}{L_2 - L_1} \right)^2 - 2 \left(\frac{s - L_1}{L_2 - L_1} \right)^3 \right\},$$

$$V(s) = V^*(s),$$

$$V(s) = V^*(s) \left\{ 1 - 3 \left(\frac{s - L_3}{L_4 - L_3} \right)^2 + 2 \left(\frac{s - L_3}{L_4 - L_3} \right)^3 \right\}$$

$$V(s) = 0,$$

(11),

where some of the parameters $f_2, f_3, L_i, i = 1, \dots, 4$ are fixed, while the others are specified in the optimization process. For 2D problems it is assumed that $v(s) = V(s)$. Since $\left. \frac{\partial V(s)}{\partial s} \right|_{s=L_1, L_4} = 0$ holds true, at these points the pressure is zero and their derivatives also vanish, so there are no singular

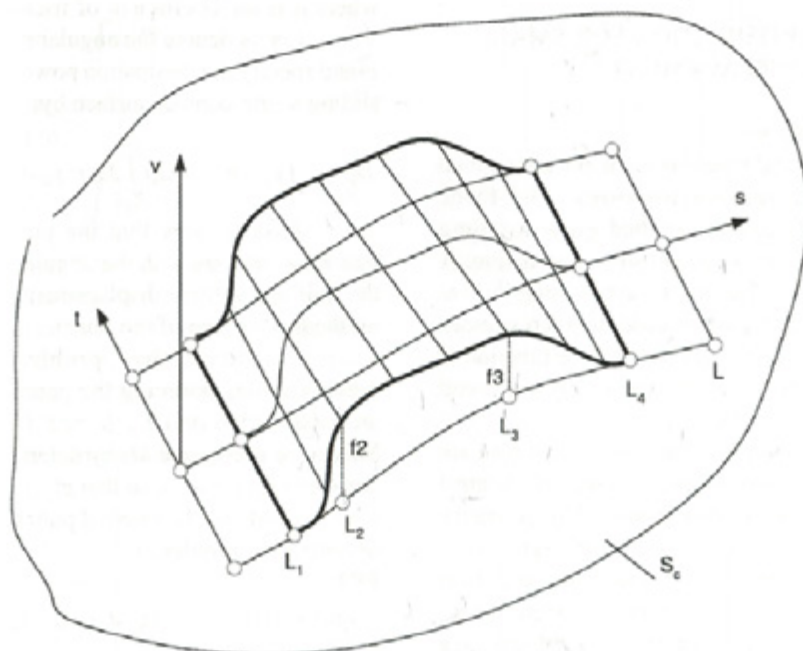


Fig. 2. Control function

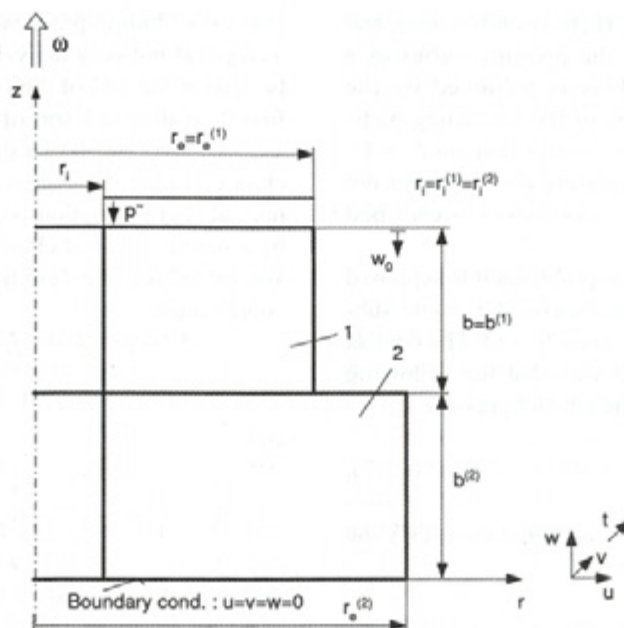


Fig. 3. The geometry of the punch problems

values in the stress distribution. In the 3D problems in paper [24] it is supposed that the upper body has a rigid translation and rotation, Ω_c is a line s , and the rotation vector is perpendicular to this line. The control function along direction t is $\tilde{v}(t) = 1$, i.e.

$$v(x) = V(s) \tilde{v}(t) \quad (12).$$

2 SHAPE OPTIMIZATION FOR SMALL DISPLACEMENTS

2.1 Punch problems

Axially symmetrical machine elements are applied in many industrial constructions. The force distribution between the bodies gives a strong influence on the stress state of the construction. A designer always endeavors to avoid singularities within the contact region in order to keep stresses at a lower level. If the control pressure function is used, the contact stress can be easily achieved without a stress singularity.

In our investigation the same examples are given for different object functions with the control of the contact pressure distribution. The geometry of the punch construction is shown in Figure 3.

In [6] a couple of contact-optimization problems can be found for punches. Here, some new, additional optimization problems are formulated.

2.2 Additional optimization problems

In engineering practice rotating particles usually transmit torque. The torque is defined as:

$$M_T = \mu \int_{r_i}^{r_o} 2\pi r^2 p_n dr \quad (13),$$

where μ is the coefficient of friction.

Let us denote the angular punch velocity by ω and specify the dissipation power due to frictional sliding at the contact surface by:

$$D_F = \int_{S_c} \tau_n \cdot \dot{u}_r = \omega \mu \int_{r_i}^{r_o} 2\pi r^2 p_n dr = M_T \omega \quad (14).$$

Assume now that the punch rotates with respect to its axis with the angular velocity ω , and the uniform vertical displacement w_0 is prescribed on the top surface of the punch.

Consider the problem of torque maximization, assuming the parameters L_1 and L_2 are unspecified and L_3 , L_4 and $L_2 - L_1$ are fixed. Maximize the torque M_T by determining the initial gap function $g = g(s)$, so that $g(s_*) = g_{\min} = 0$, where $s = r - r_i$ and r_i is the internal punch radius, thus the optimization problem is

PPI :

$$\max_{g(s), L_1} \left\{ M_T \mid p_n \geq 0, d = 0, g_{\min} = 0, \right. \\ \left. \chi = \chi(s, p_n, L_1) = 0, \sigma_e \leq \sigma_u \right\} \quad (15).$$

In order to minimize the dissipation power or torque, assume that $L_1 = 0$, $L_2 = 0$ and $L_4 - L_3$ are fixed; however, L_4 and L_3 may vary. The optimization problem is now formulated as follows **PP2** :

$$\min_{g(s), L_4} \left\{ D_F \mid p_n \geq 0, d = 0, g_{\min} = 0, \right. \\ \left. \chi = \chi(s, p_n, L_4) = 0, \sigma_e \leq \sigma_u \right\} \quad (16).$$

Using the optimization problems **PP1** and **PP2** different initial shapes of the punch surface are obtained.

2.3 Investigation of the wear process

Sliding particles that are in contact are continuously losing some material, i.e., wear occurs. Practically, it is important to know the rate of wear and the contact-pressure distribution during the wear process. When steady-state occurs during operation the information about the shape of the bodies and the stress distribution between them is significant.

Firstly, let us formulate the problem of the minimization of the wear volume rate at the contact interface. Assuming the specific wear rate \dot{w} to be dependent on contact pressure, the relative slip velocity $v_r = \|\mathbf{u}_r\|$ and the contact shear stress $\tau_n = \|\boldsymbol{\tau}_n\|$, i.e. $\dot{w} = \dot{w}(p_n, \|\mathbf{u}_r\|, \|\boldsymbol{\tau}_n\|)$, the total wear volume rate is:

$$\dot{W} = \int_{S_c} \dot{w} dS \quad (17)$$

and the wear dissipation power at the contact surface S_c is equal to:

$$D_w = \int_{S_c} p_n \dot{w} dS \quad (18).$$

The optimization problem can now be formulated as follows. Assume that the punch rotates with respect to its axis with the angular velocity ω , and the uniform vertical traction $\sigma_z = -\bar{p}$ is exerted on its top boundary with the resulting force $F_0 = \pi(r_c^2 - r_i^2) \bar{p}$. Then the gap function must be determined in order to minimize \dot{W} or D_w , thus

PP3 :

$$\min \left\{ \dot{W}, D_w \mid p_n \geq 0, \right. \\ \left. d = 0, F_p - F_0 = 0, \right. \\ \left. \chi = \chi(s, p_n, L_4) = 0, g_{\min} = 0 \right\} \quad (19),$$

where $F_p = 2\pi \int_{r_i}^{r_c} p_n r dr$ is the contact force.

Assume that the wear rule satisfies the modified Archard law [25]:

$$\dot{w} = \beta (\mu p_n)^b v_r^a = \beta \mu^b p_n^b v_r^a = \tilde{\beta} p_n^b v_r^a \quad (20),$$

where a, b, β are the wear parameters, μ is the friction coefficient, p_n is the contact pressure, $\tilde{\beta} = \beta \mu^b$, and the relative velocity is $\|\mathbf{u}_r\| = v_r = r\omega$. The shearing stress in the contact surface τ_n calculated from the contact pressure by the Coulomb dry friction law is $\tau_n = \mu p_n$.

In [18] it is demonstrated that the wear dissipation power at the contact surface is minimal in the steady state of the wear process and corresponds to the uniform wear rate. However, the minimization of the wear volume rate and the friction dissipation power is not suitable for describing the steady-state wear process.

Using the minimum of the wear dissipation power the contact pressure is:

$$p_n = \frac{F_0}{I_{D_w}} r^{-\frac{1}{b}}, \text{ where } I_{D_w} = 2\pi \int_{r_i}^{r_c} r^{1-\frac{1}{b}} dr \quad (21).$$

The wear rate is uniform along the radius

$$\dot{w} = \left(\frac{F_0}{I_{D_w}} \right)^b \tilde{\beta} \omega^a = const \quad (22).$$

The wear volume rate is

$$\dot{W} = \int \dot{w} dS = 2\pi \int_{r_i}^{r_c} \tilde{\beta} \omega^a \left(\frac{F_0}{I_{D_w}} \right)^b r dr \\ = \tilde{\beta} \omega^a \left(\frac{F_0}{I_{D_w}} \right)^b S_c = \dot{W}_{D_w} \quad (23).$$

When the upper body, e.g., a disc brake of a vehicle, is a segment of a rotationally symmetrical body with angle Φ , then Equations to remain valid, replacing I_{D_w} with $I_{D_w}^{(\Phi)}$:

$$I_{D_w}^{(\Phi)} = \Phi \int_{r_i}^{r_c} r^{1-\frac{1}{b}} dr \quad (24).$$

PP4 : Here the optimization problem is the following:

$$\min \left\{ D_w \mid p_n \geq 0, d = 0, F_p - F_0 = 0, \right. \\ \left. \chi = \chi(r, p_n) = \frac{F_0}{I_{D_w}^{(\Phi)}} r^{-\frac{1}{b}} - p_n = 0, \right. \\ \left. g_{\min} = 0 \right\} \quad (25)$$

from which the shape of the bodies belonging to the steady state can be determined.

The importance of these results is that the shape of the contacting bodies and the contact pressure after wear are determined in the case of steady-state processes without solving the time-dependent wear problem.

2.4 Solution of the optimization problems PP1 – PP4

After the discretization of the optimization problem a non-linear programming problem evolves, which is solved by a special iteration process. We distinguish two types of iterations. In the first one, which was introduced in [4], the optimal shape is determined with the prescribed control parameters $f_2, f_3, L_p, i = 1, \dots, 4$. The second type of iteration is an extension of the first one, with the stress constraint prescribed for the von Mises equivalent stress $\sigma_e, \sigma_e \leq \sigma_u$, where σ_u is the ultimate stress [6].

When the stress constraint $\max \sigma_e \leq \sigma_u$ is imposed at any Lobato integration points the values of the parameters assumed as fixed or specified in the first type iteration, should be updated in order to satisfy the stress constraint. Denote collectively the parameter that should be updated in the second type of iteration by f .

The "loading" process is characterized by the variable i_{step} . The value of f is calculated using the following formulae:

$$f = f_0 + \Delta f (i_{\text{step}} + 1) \quad (26),$$

where f_0 and Δf are chosen in advance. For instance, for the Problem PP1 $f = L_1, f_0 = r_e$ and $\Delta f = 0.1 \cdot (r_e - r_i)$. The optimization problem is solved by the first type of iteration at the fixed f . At each i_{step} a new shape is determined for the upper body.

The effective stress value σ_e is calculated at the Lobato integration points of the finite quadratic elements. We assume that for the value $f = f^*$ the effective stress is $\sigma_e^* < \sigma_u$ and at the next loading i_{step} the parameter $f = f^{**}$ and the effective stress exceeds the ultimate value $\sigma_e^{**} > \sigma_u$.

The optimal value of $f = f^{\text{opt}(i)}$ is searched for in the interval $f^* < f^{\text{opt}(i)} < f^{**}$ using the following linearization process:

$$f^{\text{opt}(i)} = f^* + (f^{**} - f^*) \frac{\sigma_u - \sigma_e^*}{\sigma_e^{**} - \sigma_e^*}, \quad (27),$$

where $f^{*(0)} = f^*, \sigma_e^{*(0)} = \sigma_e^*$. At each step of the

second type of iteration the contact shape is specified in the first iteration-based process. The second type of iteration proceeds until

$$\frac{|\sigma_u - \sigma_e^{**}(i)|}{\sigma_u} \leq 0.01 \quad (28).$$

2.5 Example for PP1

The following material parameters are assumed: Young's modulus $E = 2 \cdot 10^5$ MPa, Poisson's ratio $\nu = 0.3$, ultimate stress $\sigma_u = 250$ MPa and friction coefficient $\mu = 0.25$.

The geometrical parameters are defined as $r_i^{(1)} = r_i^{(2)} = r_i = 20$ mm, $r_e^{(1)} = 120$ mm, $r_e^{(2)} = 140$ mm, $b^{(1)} = b^{(2)} = b = 50$ mm (see Figure 3). The boundary conditions are prescribed as follows: the cylindrical surfaces $r = r_i$ and $r = r_e^{(\alpha)}$ are traction free $t_0^{(\alpha)} = \mathbf{0}$, the bottom surface $z = 0$ of the body B_2 is constrained, $u = v = w = 0$ and at the upper surface $z = 2b$ of punch B_1 is loaded by the axial displacement w_0 and is subjected to the rotational motion $v = r\alpha$.

The value of w_0 , which is the prescribed displacement of the upper body, is determined in order to achieve the same specific strain in the cylindrical bodies with the height of $b^{(1)} + b^{(2)}$. It means that:

$$\frac{100 w_0}{b^{(1)} + b^{(2)}} = 0.1\%.$$

If the radius of the cylindrical bodies is the same and the Young's modulus $E = 2 \cdot 10^5$ MPa then this specific strain will produce a 200 MPa compressive stress. Since the outer radius of the lower body is greater than the upper body's, i.e., $r_e^{(2)} = 140$ mm $>$ $r_e^{(1)}$, the stress distribution shows a singularity in the $(r_e^{(1)}, b^{(2)})$ position. The aim of the optimization is to avoid this singularity, which can be achieved by using the C^1 continuous control function defined by (10) to (12).

Using the iteration defined under Section 2.4 the problem PP1 is solved and the results of these solutions are summarized in Table 1. The results are calculated for different values of $b = b^{(1)} = b^{(2)}$.

In order to obtain very accurate results a graded mesh in geometric progression is applied along the direction z with the common factor 0.15 [7]. In direction r , both sides of the contact bordering small elements are given with the size $L_2 - L_1$. Due to re-meshing, the oscillation of stresses does not occur. The polynomial order of the finite elements is $p = 8$.

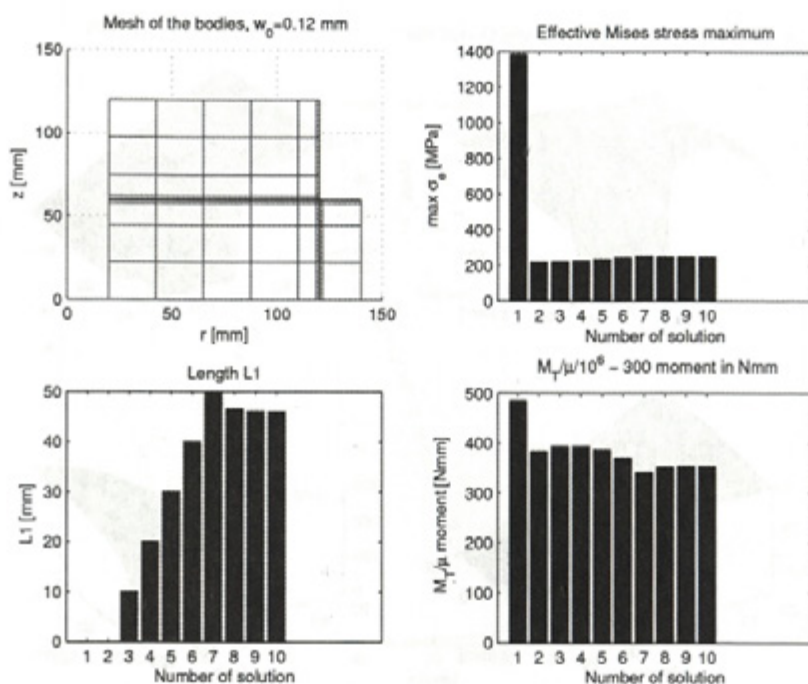


Fig. 4. Numerical results of PPI optimization with A geometry

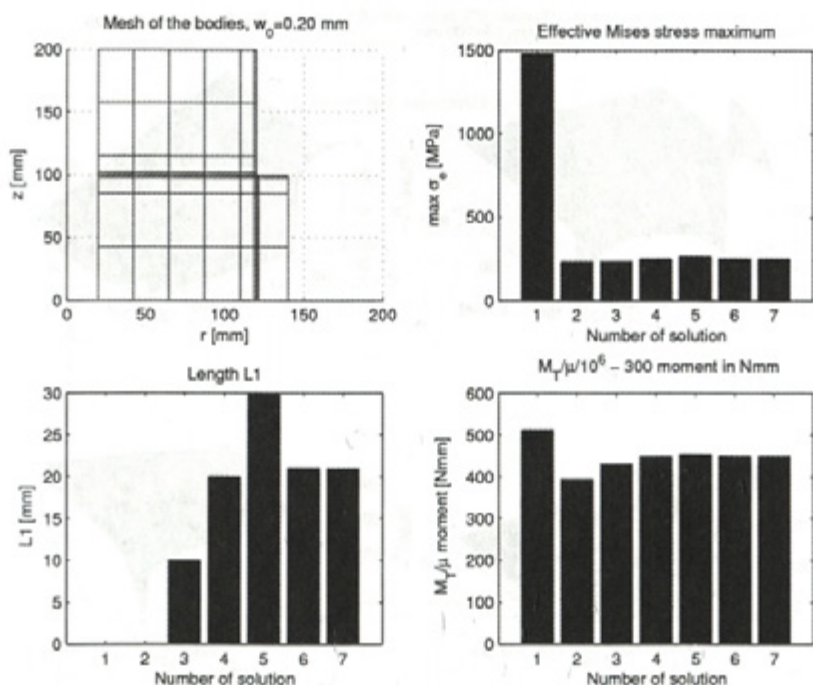


Fig. 5. Numerical results of PPI optimization with B geometry

From Table 1 it is clear that for lower values of b and w_0 in case of $\max M_T$ the maximum of the equivalent stress is lower than the ultimate stress, i.e., $\sigma_{\max} < \sigma_u$ and the condition $\sigma_{\max} = \sigma_u$ is ensured only by increasing the distance L_1 , but it results in

a lower torque between the contacting bodies.

It is also obvious that for the original construction (without optimization) the σ_{\max} is substantially over the allowed value of σ_u , which means, in practice, the yielding of the material.

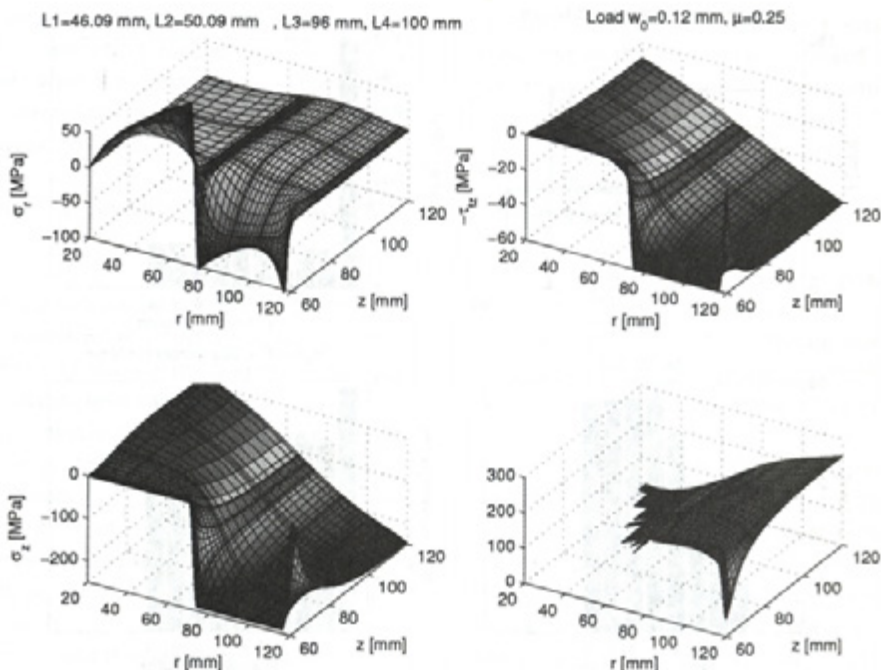


Fig. 6. Stress distribution of PPI optimization for the A geometry

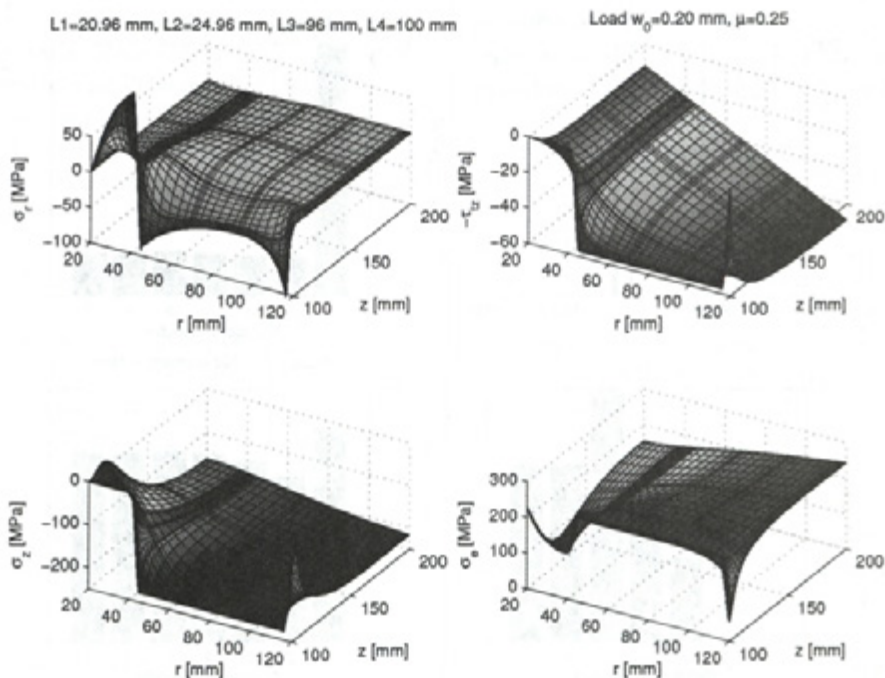


Fig. 7. Stress distribution of PPI optimization for the B geometry

In Figures 4 and 5 the finite-element mesh and the values of L_1 and M_T/μ during the iteration are illustrated. The resulting stress states are shown in Figures 6 and 7, with σ_r as the radial stress; τ_{rz} as the tangential shear stress, σ_z as the normal stress

and σ_e as the equivalent stress (Mises type). The tangential stress onto the lower surface of the upper body is defined as $|\tau_{rz}| = \mu |\sigma_z|$ according to Coulomb's law of dry friction. The top surface of the upper body has a rigid-body-like displacement.

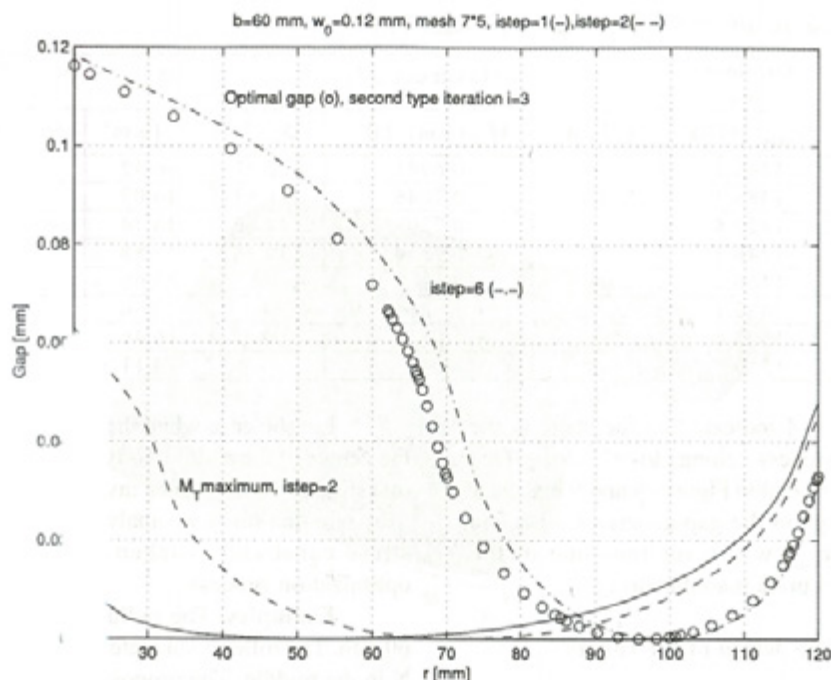


Fig. 8. Gap (shape) evolution for the A geometry

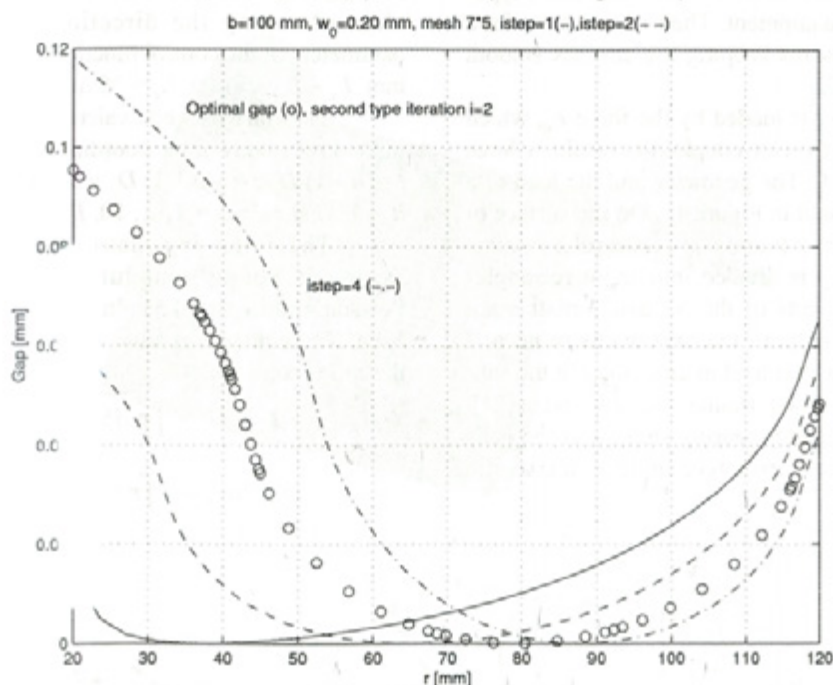


Fig. 9. Gap (shape) evolution for the B geometry

Increasing the value of b on the top surface, using St. Venant's theory, there is a linear distribution in the radial direction.

The optimal shapes of the lower edge of the upper body are drawn in Figures 8 and 9. This shape

represents the initial gap function between the contacting bodies. The definition of $\text{istep} = i_{\text{step}}$ can be found in Section 2.4. The curve designated by o belongs to the solution that is fulfilled by the additional condition $\sigma_{\text{max}} = \sigma_v$. The labels istep

Table 1. Numerical results of the optimization problem **PPI**

b	w ₀	Original	By Maximum M _T			σ _{e max} = σ _u = 250 MPa	
		Const.	L ₁ [mm]	M _T [mm] · 10 ⁻⁹	σ _{e max}	L ₁ [mm]	M _T [mm] · 10 ⁻⁹
50	0.10	1340.2	10	0.6941	222.27	56.82	0.5930
60	0.12	1386.3	10	0.7046	221.53	46.09	0.6629
70	0.14	1420.4	20	0.7209	234.76	38.74	0.7048
80	0.16	1446.3	20	0.7354	239.58	33.88	0.7317
90	0.18	1466.4	-	-	-	25.66	0.7510
100	0.20	1482.1	-	-	-	20.96	0.7599
120	0.24	1503.8	-	-	-	16.46	0.7707
140	0.28	1516.9	-	-	-	14.11	0.7791

= 6 and *istep* = 4 indicate that the stage in the iteration-based process belongs to σ_e^{**} > σ_u (see Section 2.4). To resemble Figures 8 and 9 it is clear that a little change in the gap generates a notable difference in σ_{e max}, which reminds one of the importance of accurate manufacturing.

2.6 Optimal shape design of the rollers

Rolling elements can be found in many types of engineering equipment. Their requirement for a long lifetime means keeping the stresses smooth and at a low value.

The roller is loaded by the force F₀, which gives a resultant vector couple: the resultant force F₀ and torque M₀. The geometry and the load of a roller can be found in Figure 10. On the surface of the half-space z = 0 and the rectangular contact region (S_{ct} × S_{cs}) is divided into small rectangles (D_t × D_s). Elements of the influence matrix are computed by applying the unit-intensity normal load or the tangential load in direction t in the sub-region (D_t × D_s). The formulae can be found in [27]. In order to eliminate shearing stresses at the ends of the roller the mirror technique is taken into account.

For the case when the load is not applied to the center of the roller two types of problems were investigated in an earlier investigation [13].

In this study we analyzed the case when the stress constraint is taken into account in the optimization process.

Examples. The radius of the roller is R₀ = 60 mm. The roller is subjected to loads of F₀ = 5000 N in the middle. The proposed contact region (1 × 35 mm) is divided into *kt*-*ks* = 40 × 100 rectangular elements along the directions *t* and *s*. The parameters of the control function are L₁ = 0, L₂ = 5 mm, L₄ - L₃ = 5 mm, L₄ = 35 mm, f₂ = f₃ = 0.

The von Mises equivalent stress is calculated in the lower body at the coordinates s = (is - 1) · D_s, t = (it - 1) · D_t, z = -(is - 1) · D_s, where is = 1, ..., ks + 1; it = 1, ..., kt + 1; iz = 1, ..., 10, D_s = 0.025 mm.

The following material parameters are assumed: Young's modulus E = 2 · 10⁵ MPa, Poisson's ratio ν = 0.3, ultimate stress σ_u = 250 MPa. The equations of the equilibrium related to the roller are:

$$\begin{aligned}
 \mathbf{f} &= \mathbf{f}_0 - \int_{\Omega} \mathbf{p} \, dS = 0 \\
 \mathbf{m} &= \mathbf{m}_0 - \int_{\Omega} \mathbf{r} \times \mathbf{p} \, dS = 0
 \end{aligned}
 \tag{29}$$

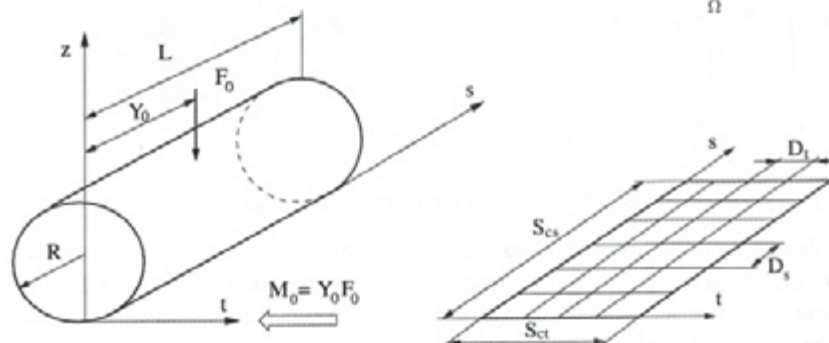
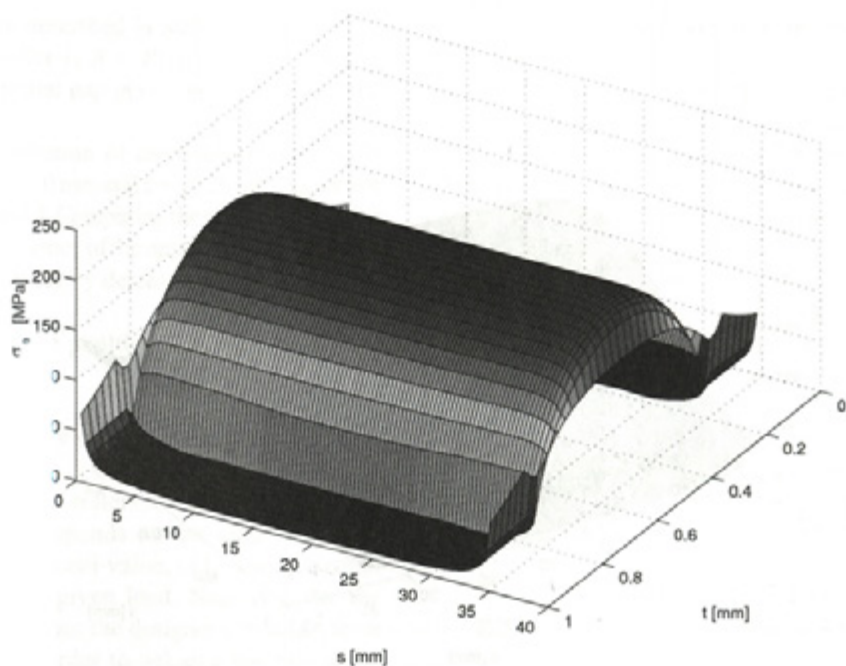
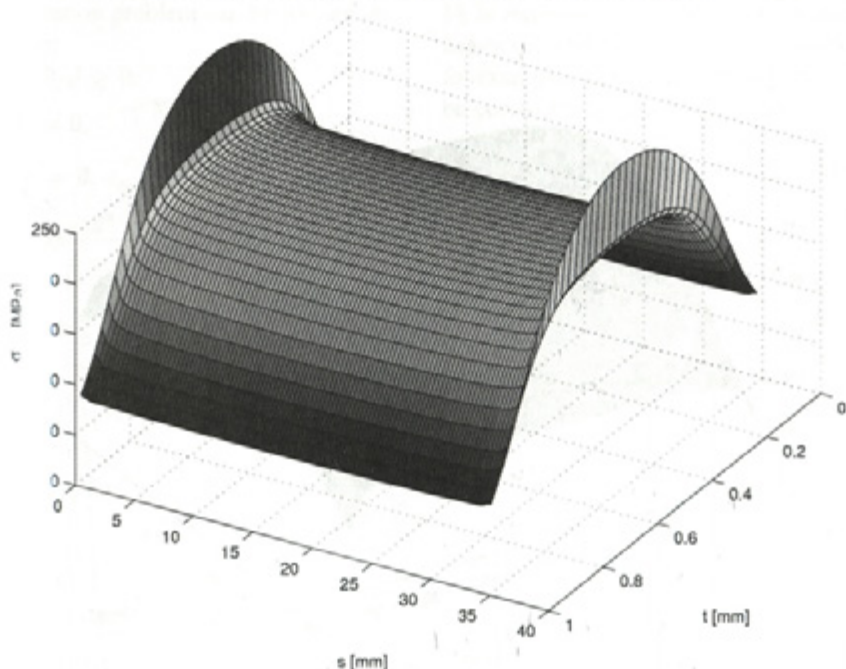


Fig. 10. The roller's load and geometrical properties

Fig. 11. Equivalent stress distribution at $z = 0$ mmFig. 12. Equivalent stress distribution at $z = 0.15$ mm

where \mathbf{r} is the position vector, \mathbf{p} is the vector of contact stress, \mathbf{f}_0 is the resultant force and \mathbf{m}_0 is the moment of the external load.

The distributions of the equivalent stress σ_e at $z = 0$ and its maximum value are found at $z = -0.15$ mm, as shown in Figures 11 and 12.

In the optimization process the lengths L_2 and L_3 are calculated because the control function is symmetrical, i.e., $\Delta L = L_2 - L_1 = L_4 - L_3$, and $L_1 = 0$, $L_4 = S_{\sigma} = 35$ mm. The control function is calculated using Equations (10) to (12).

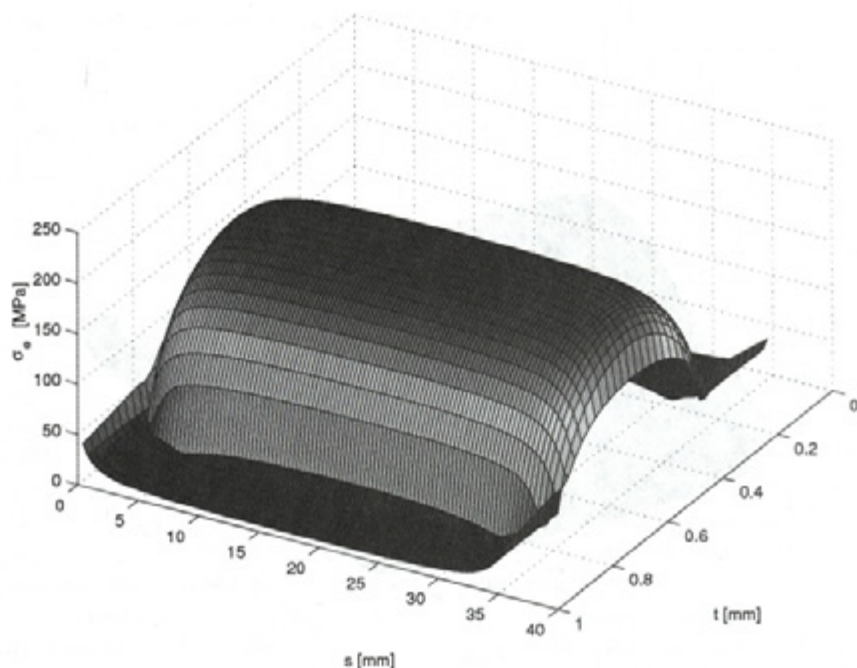


Fig. 13. The equivalent stress distribution at $z = 0$ mm after optimization

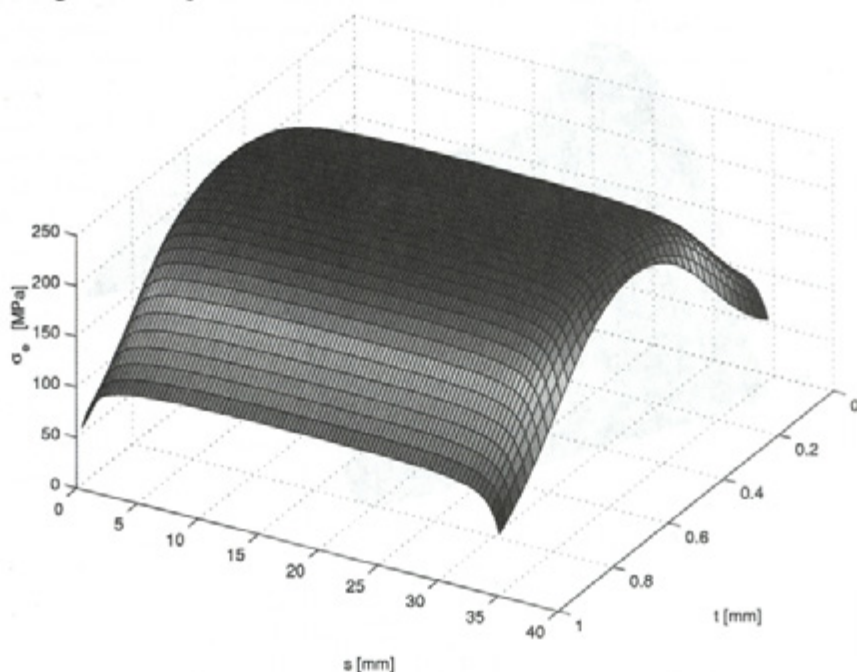


Fig. 14. The equivalent stress distribution at $z = -0.25$ mm after optimization

2.6.1 Optimization problem at a given load

The optimization problem at a given load is formulated as:

$$\min_{\Delta L} \left\{ \begin{array}{l} \sigma_{e_{\max}} \\ p_n \geq 0, d \geq 0, \\ p_n d = 0, \chi \geq 0, \end{array} \right. x \in \Omega, \quad (30)$$

$$f = 0, m = 0, \sigma_{e_{\max}} \leq \sigma_u \quad]$$

from which $\Delta L = 3.5$ mm is obtained.

Therefore, the solution is $L_2 = 3.5$ mm and $L_3 = 31.5$ mm. The minimization problem is solved by using the above-mentioned iteration process,

which is briefly described in Sub-section 2.4. The radius of the roller is $R = R(s)$, which is used to determine the initial gap $g(x) = g(s, t)$ between the bodies.

The distribution of the equivalent stress is demonstrated at $z = 0$ mm and $z = -0.25$ mm, as shown in Figures 13 and 14. Comparing the stresses in Figures 12 and 14, the influence of the optimization is obvious, i.e., σ_{\max} is significantly decreased.

2.6.2 Optimization problem for calculating the loadability

From the previous optimization problem the stress equality $\sigma_{\max} = \sigma_u$ can be achieved by different rounding-offs of the rollers at different loads, i.e., the rounding-off depends on the load. Since the control function is a uni-value, only a unique roller shape exists for a given load. Namely, after the numerical calculations the designer can select from the round-offs in order to achieve the maximum loadability.

The optimization problem can be written in the following form:

$$\max \left\{ \begin{array}{l} F_0 \mid p_n \geq 0, d \geq 0, \\ p_n d = 0, \quad \chi \geq 0 \quad x \in \Omega \end{array} \right. \quad (31).$$

$$f = 0, m = 0, \sigma_{\max} \leq \sigma_u \}$$

For the different load levels the change in radius along the roller axis can be seen in Figure 15 and 16.

The load value for a different geometry (problem) is demonstrated in Figure 17. The calculation was made with different meshes (kt, ks). The modification of the mesh does not affect the results. In all cases $L_1 = 0, L_4 = 36$ mm and because of the symmetry $L_1 = L_4 - L_2$, the change in L_2 influences the loadability.

On the basis of the numerical results the round-off obtained for the third problem (see Fig. 17) provides the best performance for high loads.

The loadability in the case of constant pressure along the meridian is approximately 4850 = 4900 N (case No. 1), while in the case of problem No. 12, because of the 5.5-mm-long transition cubic section the loadability is only = 4650 N.

3 CONTACT WITH A LARGE DISPLACEMENT AND DEFORMATION

In this section the air-spring shown in Figure 18 is analyzed. Air-springs are frequently used in heavy vehicles because of their favorable features, for example, the nonlinear spring characteristics can be controlled by the inflation pressure.

The designer is interested in having a computational tool that helps in analyzing an air-

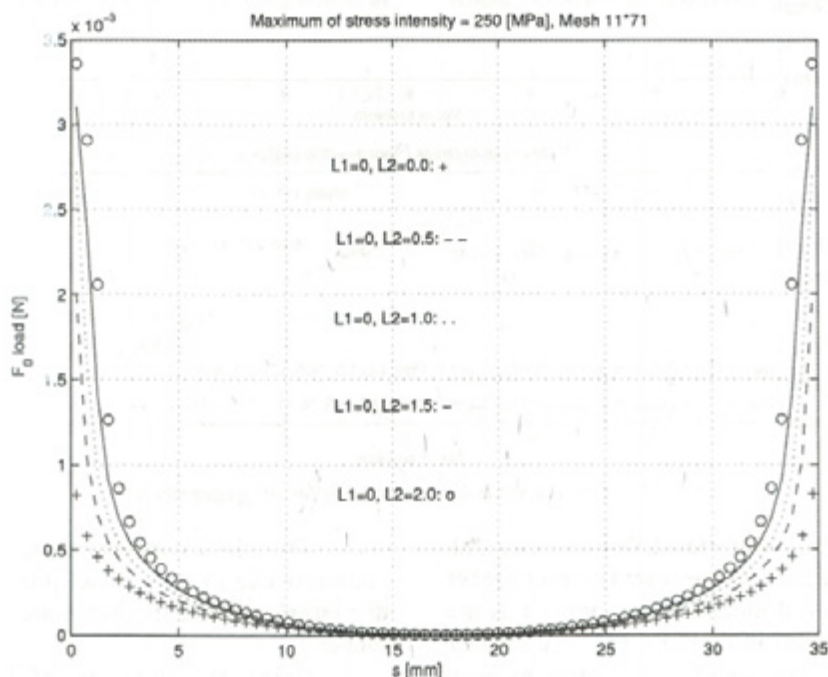


Fig. 15. Gap along the roller axis at different round-offs

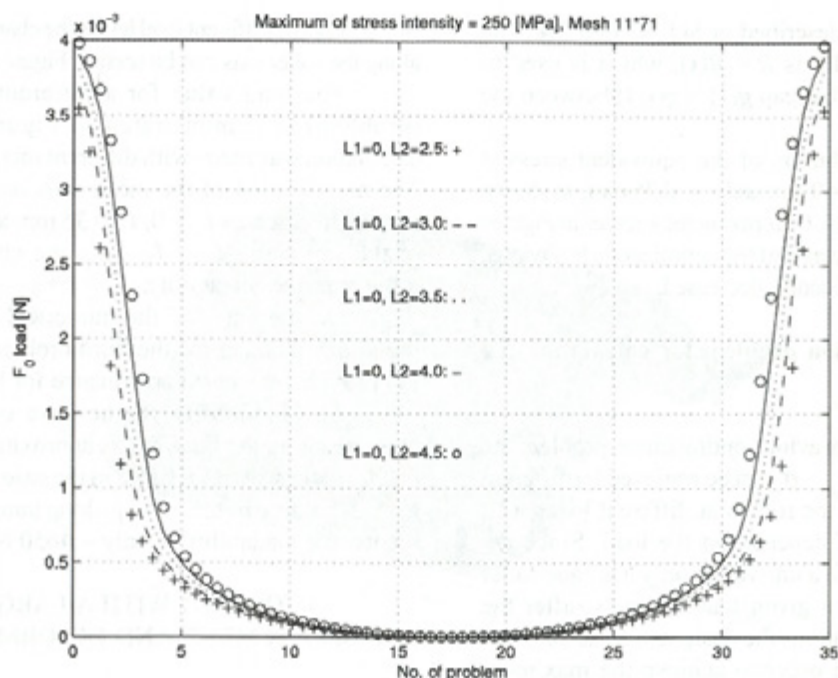


Fig. 16. Gap along the roller axis at different round-offs

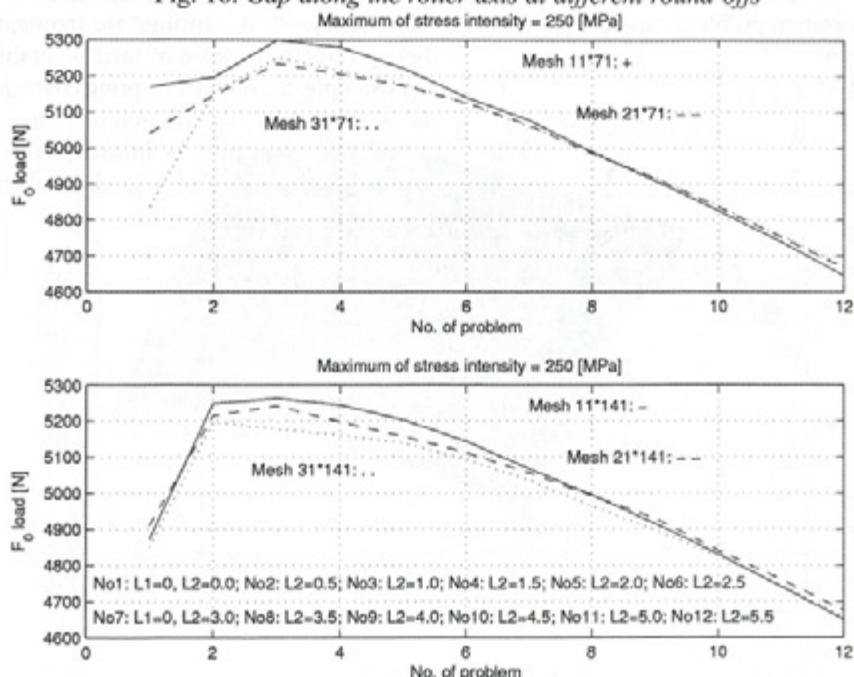


Fig. 17. Load distribution versus different geometries

spring before it is manufactured. One can determine its spring characteristics, the quantitative influences of the geometrical modifications, as well as the stresses and strains in the fiber-reinforced rubber composite. A finite-element program has been developed, which is based on the following theory.

The axially symmetrical problem is strongly nonlinear due to the contact problem, the large displacements and the incompressibility of the rubber.

Using the notation of Figure 1 the deformation gradient tensor is given as:

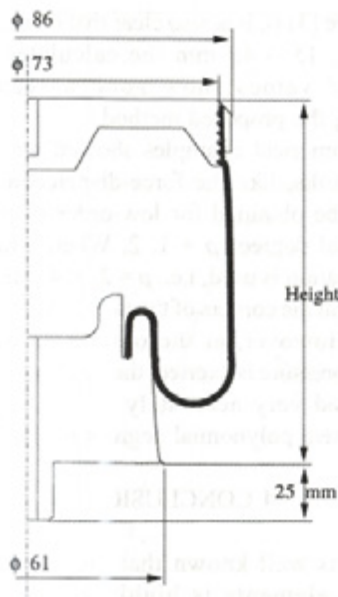


Fig. 18. Cross-section of the air-spring

$$\mathbf{F}^\alpha = \frac{\partial \mathbf{x}^\alpha}{\partial \mathbf{X}^\alpha} \quad (32),$$

where \mathbf{X}^α denotes the undeformed configuration, while \mathbf{x}^α belongs to the current configuration. In the examined problem the lower body is a rigid one; therefore, $^\alpha$ will be omitted in the following.

In order to treat the incompressibility condition we introduce the deformation gradient in a decomposed form:

$$\mathbf{F} = \mathbf{F}_{Vol} \hat{\mathbf{F}} \quad (33),$$

where the volumetric part of the deformation gradient is defined as:

$$\mathbf{F}_{Vol} = J^{1/3} \mathbf{I} \quad (34),$$

where \mathbf{I} is the unit tensor. The deviatoric part of the deformation gradient is obtained as:

$$\hat{\mathbf{F}} = J^{-1/3} \mathbf{F} \quad (35),$$

and the volumetric change is:

$$J = \det \mathbf{F} \quad (36).$$

The incompressibility condition is fulfilled when $J = 1$.

In our investigation the rubber ($\beta = 1$) is assumed to be a nearly incompressible material and

it is modeled with the Hu-Washizu functional, see [26], and the fiber-reinforced layer ($\beta = 0$) is homogenized by the so-called Halpin-Tsai equations [28]:

$$\Pi_{HW}(\mathbf{u}, \bar{J}, \bar{p}) = \beta \left\{ \int_V \widehat{W}(\mathbf{C}) dV + \int_V U(\bar{J}) dV \right. \\ \left. + \int_V \bar{p}(J - \bar{J}) dV - \int_{S_i} \mathbf{u} \cdot \mathbf{n} \bar{p} dA \right\} + \\ + (1 - \beta) \frac{1}{2} \int_V \mathbf{E} \cdot \mathbf{D} \cdot \mathbf{E} dV \quad (37),$$

where ' $\cdot \cdot$ ' means the double dot product of two tensors, \bar{p} is the prescribed pressure and \widehat{W} is the Mooney-Rivlin strain energy density:

$$\widehat{W}(\mathbf{C}) = \mu_{10} (\hat{I}_{1\hat{C}} - 3) + \mu_{01} (\hat{I}_{2\hat{C}} - 3). \quad (38)$$

in which μ_{01}, μ_{10} are the Mooney-Rivlin constants, invariants of the Cauchy-Green strain tensor:

$$\hat{I}_{1\hat{C}} = \hat{C}_{11} + \hat{C}_{22} + \hat{C}_{33} \quad (39)$$

$$\hat{I}_{2\hat{C}} = \frac{1}{2} (\hat{I}_{1\hat{C}}^2 - \hat{C} \cdot \hat{C}) \quad (40)$$

and the Cauchy-Green strain tensors are defined by the different deformation tensors

$$\hat{\mathbf{C}} = \hat{\mathbf{F}}^T \hat{\mathbf{F}} \quad (41),$$

where T denotes the transpose of a tensor,

$$\mathbf{C} = \mathbf{F}^T \mathbf{F} \quad (42).$$

The II. Piola-Kirchhoff stress tensor for the rubber is given by:

$$\mathbf{S} = 2 \frac{\partial \widehat{W}}{\partial \mathbf{C}} + \bar{p} \mathbf{C}^{-1}$$

and the fiber-reinforced layer is assumed to be linear

$$\mathbf{S} = \mathbf{D} \cdot \mathbf{E} \quad (43),$$

where \mathbf{D} is the constitutive tensor and \mathbf{E} is the Green-Lagrange strain tensor

$$\mathbf{E} = \frac{1}{2} (\mathbf{F}^T \mathbf{F} - \mathbf{I}) \quad (44).$$

The incompressibility is enforced by a penalty function, as was proposed by [29]:

$$U(\bar{J}) = \frac{\kappa}{50} (\bar{J}^5 + \bar{J}^{-5} - 2).$$

The finite-element computations were performed by p -extension elements. The

polynomial degrees of the displacements were chosen as $p = 1, \dots, 4$, while the independently approximated volumetric change \bar{J} and the hydrostatic pressure \bar{p} were approximated with an order of one degree lower than the displacement according to [30].

The contact problem is treated with a simplified approach. The contacting boundary is approximated by a polygon, i.e., the edge of the contacting element is forced to be a straight line, also when a high-order displacement approximation is used. In practice, three-node contact elements were implemented, as detailed in [22].

The fiber-reinforced rubber composite consists of four layers, i.e., a rubber inner liner, a rubber outer cover and two homogenized orthotropic fiber plies, which are oriented at angles of $\pm 45^\circ$. The thicknesses of the rubber layers and the fiber plies are 1 mm and 0.5 mm, respectively. The inflation pressure is $\bar{p} = 4 \text{ bar}$. The finite-element computations simulate the working process of the air-spring. Assuming a constant inflation pressure the deformations, stresses and resultant forces were determined in 19 positions.

Three deformed shapes, i.e., the 1st, 10th, 19th of the airspring are shown in Figure 19.

The vertical displacement versus the resultant force curve, i.e., the characteristic curve, is shown in Figure 20, together with the measured

values (see [31]). It is also clear that on the working area, i.e., 15 – 45 mm the calculated and the measured values show good agreement, so validating the proposed method.

Numerical examples showed that accurate global results, like the force-displacement curve, can also be obtained for low-order displacement polynomial degrees $p = 1, 2$. When a high-order approximation is used, i.e., $p = 2, 3, 4$, stress peaks may arise at the corners of the polygon of the contact border. However, at the other side where the inflation pressure is exerted, the boundary condition is satisfied very accurately for the high-order displacement polynomial degrees $p = 3, 4$.

4 CONCLUSIONS

It is well known that the stress state of machine elements is highly sensitive to the geometry near the stress peaks. This is a requirement to avoid stress peaks. The second section of the article shows an effective method for accomplishing it. Namely, a smooth contact-pressure distribution can be achieved by using an appropriate *control function* on the controlled sub-domain.

Highly accurate results may be realized using p -extension finite elements for the solution of the contact problems, combined with a

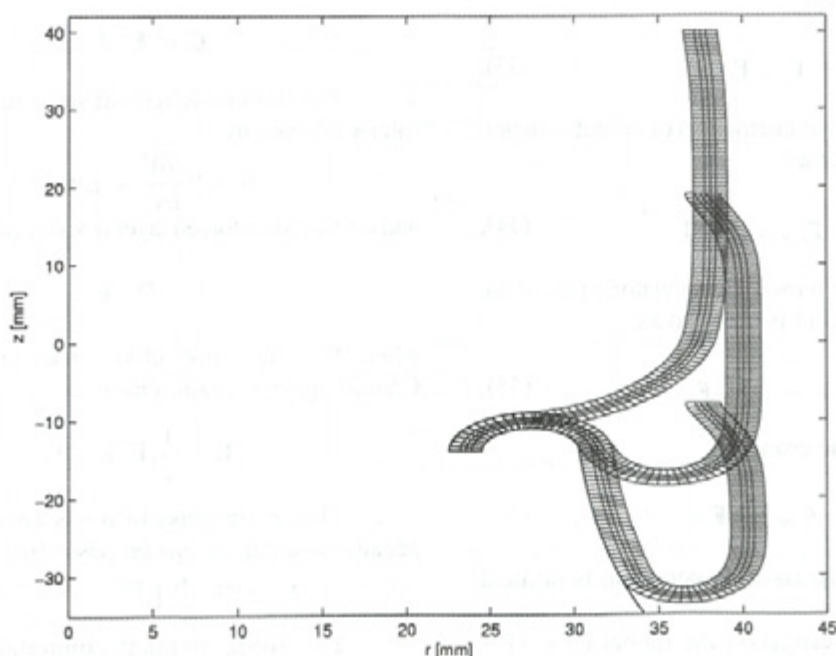


Fig. 19. Deformed shapes in three positions

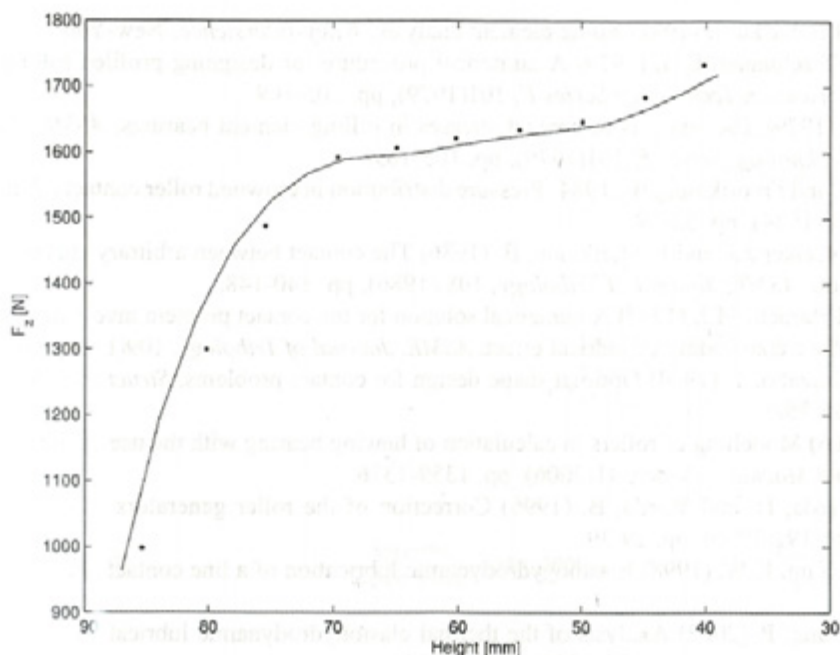


Fig. 20. Characteristic curve of the air-spring; solid line: numerical results, dots: measurements

positioning technique and special re-meshing.

The provided examples demonstrate the effectiveness of the proposed algorithms for the determination of the initial shape, i.e., the initial gap, by observing the stress constraint. The method is also applicable for designing a clutch to maximize the transmissible torque.

The applied optimization procedure is applicable for designing highly loaded rollers, which are characterized by a smooth contact-stress distribution along the contact surfaces. Two types of optimization problems were investigated. Firstly, the round-off (ΔL) is determined for a given force load (see Equation 30). Secondly, the force load is

calculated for the prescribed round-off (see Equation 31). The maximum force load can also be determined with a modification of the round-off.

The p -extension finite elements are also very applicable for large-displacement problems when the contacting element's edge is kept as a straight line. The global results are accurate enough at a low order of approximations, i.e., the measured and calculated results show good agreement.

Acknowledgment

The research is partially supported by the Hungarian Research Fund (OTKA T037759).

5 REFERENCES

- [1] Hilding, D., Klarbring, A. and Petterson, J. (1999) Optimization of structures in unilateral contact, *ASME, Appl. Mech. Rev.*, 52:(4) (1999), pp. 139-160.
- [2] Haslinger, J. and Neittaanmaki, P. (1996) Finite element approximation for optimal shape design, *John Wiley & Sons Ltd.*, London.
- [3] Goryacheva, I.G. and Dobuchin, M.H. (1998), Contact problems in tribology, *Mashinostroenie*, Moscow.
- [4] Páczelt, I. (2000) Iterative Methods for solution of contact optimization problems, *Arch. Mech.*, 52:(4-5) (2000), pp. 685-711.
- [5] Páczelt, I. and Szabó, T. (2002) Solution of contact optimization problems of cylindrical bodies using the hp-FEM, *International Journal for Numerical Methods in Engineering*, 53:(1) (2002), pp. 123-146.
- [6] Páczelt, I. and Baksa, A. (2002) Examination of contact optimization and wearing problems, *Journal of Computational and Applied Mechanics*, 3 (2002), pp. 61-84.

- [7] Szabó, B. and Babuška, I. (1991) Finite element analysis, *Wiley-Interscience*, New-York.
- [8] Oh, K.P. and Trachmann, E.G. (1979) A numerical procedure for designing profiled rolling, *ASME, Journal of Lubrication Technology Series F*, 101(1979), pp. 105-109.
- [9] Harnett, M.J. (1979) The analysis of contact stresses in rolling element bearings, *ASME, Journal of Lubrication Technology Series F*, 101(1979), pp. 105-109.
- [10] Trostenfelt, B. and Fredriksson, B. (1984) Pressure distribution in crowned roller contacts, *Engineering Analysis*, 1:(1) (1984), pp. 32-39.
- [11] de Mul, J.M., Kalker J.J. and Frederiksson, B. (1986) The contact between arbitrary curved bodies of finite dimension, *ASME, Journal of Tribology*, 108 (1986), pp. 140-148.
- [12] Chiu, Y.P. and Harnett, M.J. (1987) A numerical solution for the contact problem involving bodies with cylindrical surface considering cylindrical effect, *ASME, Journal of Tribology*, 109(1987), pp. 479-486.
- [13] Páczelt, I. and Szabó, T. (1994) Optimal shape design for contact problems, *Structural Optimization*, 7(1994), pp. 66-75.
- [14] Kania, L. (2006) Modelling of rollers in calculation of hewing bearing with the use of finite elements, *Mechanism and Machine Theory*, 41(2006), pp. 1359-1376.
- [15] Krzeminski-Freda, H. and Warda, B. (1996) Correction of the roller generators in spherical roller bearings, *Wear*, 192(1996), pp. 29-39.
- [16] Park, T.J. and Kim, K.W. (1998) Elastohydrodynamic lubrication of a line contact, *Wear*, 223(1998), pp. 102-109.
- [17] Lim, X. and Yang, P. (2002) Analysis of the thermal elastohydrodynamic lubrication of a finite line contact, *Tribology International*, 35(2002), pp. 137-144.
- [18] Páczelt, I. and Mróz, Z. (2005), On optimal contact shapes generated by wear process, *International Journal for Numerical Methods in Engineering*, 63:(9) (2005), pp. 1250-1287.
- [19] Wriggers, P. and Miehe, C. (1994) Contact constraints within thermo-mechanical analysis a finite element model, *Computer Methods in Applied Mechanics and Engineering*, 113(1994), pp. 301-319.
- [20] Podra, P. and Anderson, S. (1999) Simulating sliding wear with finite element method, *Tribol. International*, 32(1999), pp. 71-81.
- [21] Páczelt, I. and Pere, B. (1999) Investigation of contact wearing problems with hp-version of the finite element method, *Thermal Stress '99*, Skrzypek, J.J. and Hetnarski, R.B. (Eds), Crakow University of Technology, pp. 81-84.
- [22] Crisfield, M.A. (1997) Non-linear finite element analysis of solids and structures, *John Wiley & Sons*, New York.
- [23] Wriggers, P. (2002) Computational contact mechanics, *J. Wiley & Sons*, New York.
- [24] Páczelt, I., Szabó, T. and Baksa, A. (2004) Product designing using finite element method and contact optimizations, *Proceedings of the TMCE2004*, Lausanne, Switzerland, Horváth & Xirouchakis (Eds), Millpress, Rotterdam, pp. 267-276.
- [25] Archard, J.F. (1953) Contact and rubbing of flat surfaces, *Journal of Applied Physics*, 24(1953), pp. 981- 988.
- [26] Bone, J. and Wood, R.D. (1997) Nonlinear continuum mechanics for finite element analysis, *Cambridge University Press*, Cambridge.
- [27] Kalker, J.J. (1990) Three dimensional elastic bodies in rolling contact, *Academic Publisher*, Dordrecht.
- [28] Halpin, J.C. and Tsai, S.W. (1969) Effect of environmental factors on composite materials, *AFML-TR*, 1969, pp. 67-423.
- [29] Hartmann, S. and Neff, P. (2003) Polyconvexity of generalized polynomial-type hyper elastic strain energy functions for near-incompressibility, *International Journal for Solids and Structures*, 40(2003), pp. 2767-2791.
- [30] Stenberg, R. and Suri, M. (1996) Mixed hp finite element methods for problems in elasticity and Stokes flow, *Numer. Math.*, 72(1996), pp. 367-389.
- [31] Firestone Industrial Products Company, Engineering Manual & Design Guide, 2006. Available online at: www.macsspring.com/website/catalogs/design.guide.pdf (accessed 05 July 2006)

Authors' Address:

Prof. Dr. István Páczelt
Dr. Attila Baksa
University of Miskolc
Department of Mechanics
H-3515 Miskolc-Egyetemvaros, Hungary

Dr. Tamás Szabó
Szechenyi Istvan University
Department of Applied Mechanics
Egyetem ter 1
H-9028 Győr, Hungary

Prejeto: 2.5.2007
Received:

Sprejeto: 27.6.2007
Accepted:

Odprto za diskusijo: 1 leto
Open for discussion: 1 year